PHYSICAL REVIEW C **87**, 064601 (2013)

Neutron multiplicity measurements for ^{19}F + ^{194,196,198}Pt systems to investigate the effect of shell closure on nuclear dissipation

Varinderjit Singh, B. R. Behera,[*] Maninder Kaur, and A. Kumar
Department of Physics, Panjab University, Chandigarh 160014, India

P. Sugathan, K. S. Golda, A. Jhingan, M. B. Chatterjee, and R. K. Bhowmik[†]
Inter University Accelerator Centre, New Delhi 110067, India

Davinder Siwal and S. Goyal
Department of Physics and Astrophysics, Delhi University, Delhi 110007, India

Jhilam Sadhukhan[‡]
Department of Physics and Astronomy, University of Tennessee, Knoxville, Tennessee 37996, USA and
Physics Division, Oak Ridge National Laboratory, Oak Ridge, Tennessee 37831, USA

Santanu Pal
Variable Energy Cyclotron Centre, 1/AF, Bidhan Nagar, Kolkata 700064, India

A. Saxena, S. Santra, and S. Kailas
Nuclear Physics Division, Bhabha Atomic Research Centre, Mumbai 400085, India
(Received 27 February 2013; revised manuscript received 28 April 2013; published 3 June 2013)

Pre- and post-scission neutron multiplicities are measured for the three isotopes of Fr (^{217}Fr, ^{215}Fr, and ^{213}Fr) in the excitation energy range of 48–91.8 MeV. Out of these three isotopes, ^{213}Fr has shell closure ($N_C = 126$) while the other two are non-closed-shell nuclei. Statistical model calculations using Kramers' fission width are performed to investigate shell effects on the dissipation strength which fit the experimental data. It is observed that shell correction to the binding energies of the evaporated particles strongly affects the fitted values of the dissipation strength. However, the best-fit dissipation strength is only weakly influenced by the inclusion of shell correction in fission barrier.

DOI: 10.1103/PhysRevC.87.064601 PACS number(s): 25.70.Jj, 25.70.Gh, 24.10.Pa

I. INTRODUCTION

It is now a recognized fact that the dynamics of nuclear collective motion at temperatures of the order of a few MeV is dissipative in nature. Dissipation or viscosity in a nuclear system essentially accounts for the conversion of the collective kinetic energy to internal excitations of the system [1]. In earlier studies, a dissipative dynamics for the saddle-to-scission motion in nuclear fission was found necessary in order to explain the most probable fission fragment kinetic energies for nuclei throughout the periodic table [2,3]. The strong damping of entrance channel kinetic energy in deep inelastic collisions between two heavy nuclei also suggests the presence of dissipation in nuclear collective dynamics [4]. More recently, it was found that dissipation is required to explain a number of observables in heavy-ion-induced fusion-fission reactions including the pre-scission neutron multiplicity and the evaporation residue cross section [5]. From the analysis of a large set of experimental data [6], it was shown that a large dissipation is required to explain experimental results at compound nucleus temperatures above 1 MeV. Subsequently Thoennessen and Bertsch [7] observed a threshold behavior of dissipation from the analysis of experimental data.

Nuclear dissipation manifests itself in heavy-ion-induced fusion-fission reactions through the enhancement of pre-scission evaporation of neutrons, other light particles and photons with respect to the predictions of the standard statistical model of compound nuclear decay [8–10]. An enhancement of the evaporation residue cross section is also observed [11]. Dissipation hinders or slows down the fission process, causing a reduction of the fission width [12] and thereby causing an increase in the number of evaporated particles and γ rays prior to fission. A large number of experimental and theoretical studies have been made to identify and estimate the magnitude of nuclear dissipation in heavy-ion-induced reactions [10,13,14].

In the statistical model of compound nuclear decay, the pre-scission multiplicities of various evaporated particles depend on the Γ_i/Γ_f ratios (i and f represent the various evaporation channels and fission, respectively) at different stages of evolution of the initial compound nucleus until fission. The above ratio, in turn, depends on the density of nuclear levels, separation energies of the evaporated particles,

---

[*] Corresponding author: bivash@pu.ac.in

[†] Present address: 45C, Maharaja Tagore Road, Dhakhuria, Kolkata 700031.

[‡] On leave of absence from VECC, Kolkata 700 064, India.

the fission barrier, and the strength of dissipation. While the separation energies can be obtained from the ground-state nuclear masses, the effect of nuclear shells can be incorporated in the Fermi gas model of the level density formula and in the liquid-drop-model (LDM) fission barrier through additional terms [15]. It may, however, be mentioned here that the experimental values of the ground-state nuclear masses may not always be available and in such cases, the shell-corrected LDM mass can be used. The strength of the nuclear dissipation is yet to be firmly established, though considerable progress has been achieved in terms of understanding the origin of nuclear dissipation and its relation to nuclear shells [13,16,17]. The strength of the nuclear dissipation, therefore, is usually treated as a free parameter and its value is obtained from fitting of experimental data. It is evident that the dissipation strength thus obtained depends on the magnitudes of the other nuclear properties, viz., the separation energy, the level density, and the fission barrier used in the statistical model calculation. The following question then naturally arises. How sensitive is the best-fit value of the dissipation parameter to the choice of the above-mentioned nuclear properties? Specifically, one may like to know to what extent the shell corrections in the above nuclear properties affect the fitted values of the dissipation strength. A proper understanding of such issues is important in order to attribute the value of the best-fit dissipation parameter to the true dissipative property of the compound nucleus. Furthermore, any shell effect in dissipation is expected to be revealed in its best-fit values when shell corrections in all the other nuclear properties are accounted for in the statistical model calculation.

To study shell effects in nuclear dissipation through analysis of experimental data, we have measured the excitation function of neutron multiplicities from the three compound nuclei, ^{217}Fr, ^{215}Fr, and ^{213}Fr, produced in the ^{19}F + ^{194,196,198}Pt reactions. To get an unambiguous picture of the shell effects, the target-projectile combinations are so chosen that different isotopes of the same compound nucleus (CN) are formed. This choice is further guided by the consideration that one of the compound nuclei should be a closed-shell nucleus since shell effects are strongest at a closed shell. Of these three isotopes, ^{213}Fr has neutron shell closure ($N_C = 126$) while the other two are away from shell closure. For a better comparison of the results, the beam energies for the experiments were adjusted such that the compound nuclei in the different reactions were produced with approximately the same excitation energies.

In a previous publication [18], we presented a brief account of the experiment along with an analysis of the experimental results. The effect of shell correction in the level density and the fission barrier as reflected in the best-fit values of the dissipation parameter was investigated in some detail in Ref. [18]. It was shown that inclusion of shell effects in the level density and the fission barrier is important in order to obtain a consistent picture of nuclear dissipation. In the present work, we shall examine the role of shell correction to the ground-state nuclear mass in determining the magnitude of the fitted dissipation parameter. Specifically, we shall study how the dissipation parameter changes when LDM and shell-corrected LDM masses are used instead of experimental masses to obtain the particle separation energies for calculating the widths of the various particle evaporation channels. This issue can be important for studies of exotic or superheavy nuclei where experimental masses are not available. We shall further assess the effect of shell correction in fission barrier on the fitted values of the dissipation parameter.

The paper is organized as follows. The experimental setup is described in Sec. II, and the method of data analysis is presented in Sec III. Section IV contains the details of the statistical model calculations and comparison of experimental results with the statistical model predictions. A summary and the conclusions are presented in the last section.

II. EXPERIMENTAL SETUP

A series of experiments was performed using the National Array of Neutron Detectors (NAND) facility at Inter University Accelerator Centre (IUAC), New Delhi. A pulsed beam of ^{19}F ($E_{\text{lab}} = 92.4$–140.8 MeV) was bombarded on ^{194,196,198}Pt targets from a Pelletron + LINAC accelerator system. The targets were kept at the center of a thin walled (3 mm thick) spherical scattering chamber of 60 cm diameter at 90° with respect to the beam. The fission fragments produced in the reactions were detected in coincidence using a pair of position-sensitive multiwire proportional counters (MWPC1 and MWPC2). The central angular positions θ_{MWPC1} and θ_{MWPC2} were 35° and −125.5° with respect to the beam direction, kept at distances of 18.5 and 17 cm, respectively. MWPC1 and MWPC2 subtended opening angles of ±19°, ±11.5°, and ±20.5°, ±12.5° with respect to the central θ, ϕ angular positions, respectively. The emission angles of the fission fragments were determined in both the polar and azimuthal coordinates (θ, ϕ) with respect to the beam direction. The MWPC detectors used consist of three electrodes: an anode position wire frame to measure the horizontal (X) position, a central cathode foil, and another position wire frame to measure the vertical (Y) position. The MWPCs were operated at 3.5 torr pressure of isobutane gas with a cathode bias of −430 V while the anode was grounded. A clean separation between fission fragments and the elastically scattered beam was obtained as shown in Fig. 1.

The neutrons emitted during the reaction were detected in coincidence with the fission fragments using 24 NE213 organic liquid scintillators. Of these detectors, 16 detectors each with an active volume of 127 mm diameter × 127 mm thickness were kept in the reaction plane, and the remaining detectors each with an active volume of 76 mm diameter × 127 mm thickness were placed at ±15° with respect to the reaction plane. These detectors were kept at different angles ranging from 30° to 315° around the scattering chamber. Figure 2 shows the schematic diagram of the NAND scattering chamber and the neutron detectors.

A hardware threshold of 120 keV electron equivalent was applied to the neutron detector array by calibrating it with standard γ sources of ^{137}Cs and ^{60}Co [19]. The normalization and monitoring of the beam flux was performed using two silicon surface barrier detectors by detecting the elastically

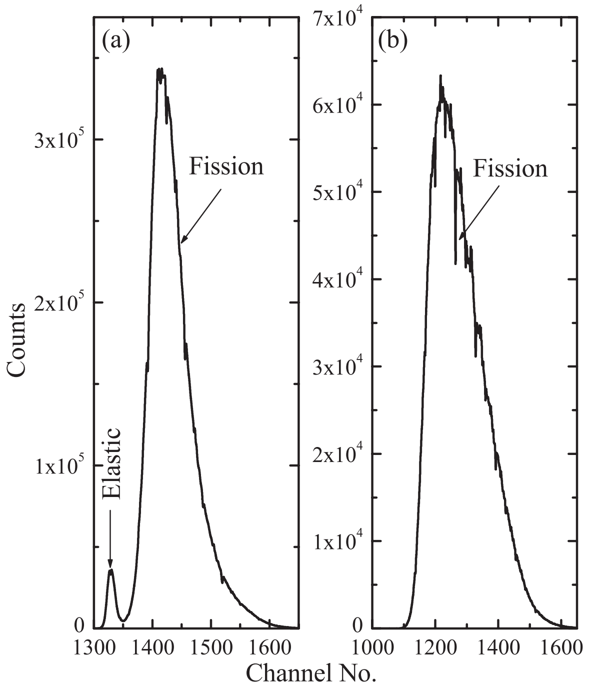

FIG. 1. Cathode spectra of both MWPCs, (a) forward detector and (b) backward detector, for $^{19}\mathrm{F} + {}^{198}\mathrm{Pt}$ reaction at 140.8 MeV of beam energy.

scattered beam particles at azimuthal angles ±16° to the beam direction out of the reaction plane. Neutrons and γs were discriminated by using both the time-of-flight technique (TOF) and the method of pulse shape discrimination (PSD) based on the zero crossover technique [20]. Figure 3 shows the TOF and PSD spectra recorded during the experiment.

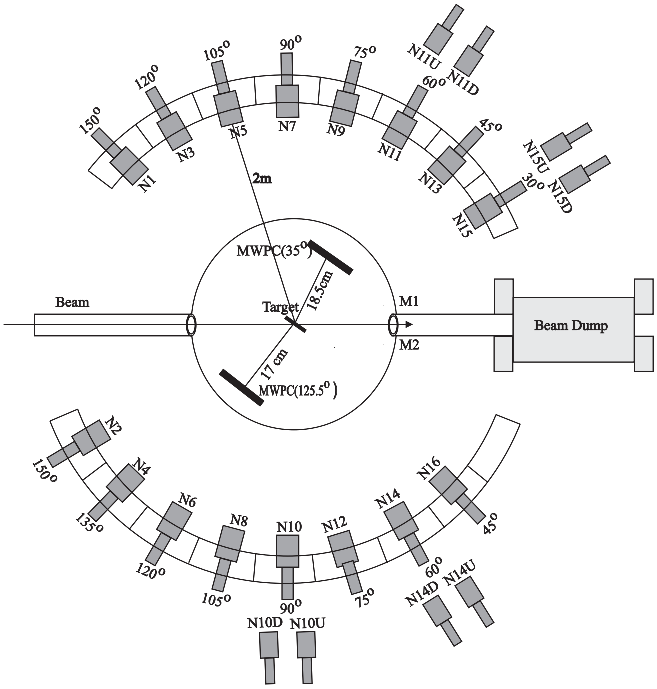

FIG. 2. Schematic diagram of the NAND setup.

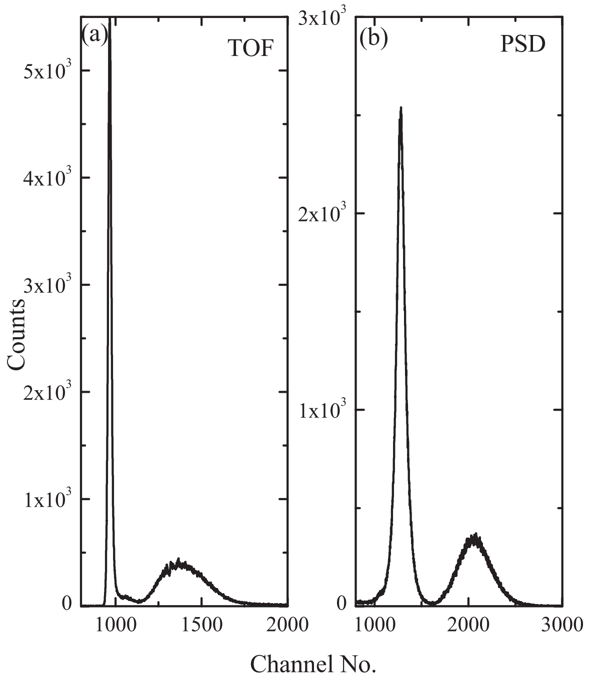

FIG. 3. Time-of-flight (TOF) and pulse shape discrimination (PSD) spectra of neutron detector.

The data acquisition system was triggered by the OR of the cathode signals of the two fission detectors ANDed with the RF of beam pulse. The ANDing with the RF of beam helped to avoid false triggering. The TOF of fission fragments and neutrons along with the positions of the fission fragments were recorded in event mode for off-line analysis. A BaF_2 detector was kept near the beam dump to monitor the beam pulsing. A time-to-amplitude converter (TAC) spectrum was generated between the BaF_2 timing and the RF of the beam pulse. The pulse width of the beam was found to be 1.2 ns for the Pelletron beam and 400 ps for the (Pelletron + LINAC) beam.

The efficiency of the neutron detectors was determined experimentally by measuring the neutron energy spectrum from a ^{252}Cf (strength 925 kBq) spontaneous fission source. The ^{252}Cf source was kept at the target position and the fission detector (MWPC) was 1.8 cm from the target position. The MWPC was operated at the same conditions as maintained during the experiment. At these operating conditions, the MWPC was not sensitive for the detection of α particles emitted by the ^{252}Cf source and had 100% efficiency for detection of the fission fragments. The TOFs were recorded using the MWPC as the common start and the neutron detectors as the stop signals.

The position calibration of the MWPCs was required to obtain full position information. The MWPCs were calibrated using ^{241}Am and ^{252}Cf radioactive sources. A mask with 1 mm diameter holes separated by 5 mm was placed in front of a MWPC. A position resolution of 1.4 mm was obtained for both the detectors. The time-to-digital converter (TDC) was calibrated using an ORTEC 462 time calibrator module.

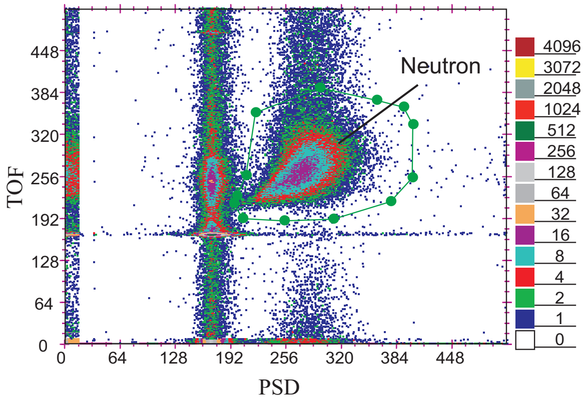

FIG. 4. (Color online) Two-dimensional plot of TOF vs PSD used to distinguish the neutrons from the γ events. The neutron lobe is marked with green dot-line marker.

III. DATA ANALYSIS

The experimental neutron detection efficiency of the neutron detectors and the neutron multiplicities for the reactions studied are extracted from the experimental data as follows.

A. Extraction of neutron detection efficiency

The TOF spectra recorded during the efficiency run are calibrated using TDC calibration and the prompt γ peak of TOF spectra as a reference. The two-dimensional neutron gate (PSD vs TOF), as shown in Fig. 4, is applied on the calibrated TOF spectra to distinguish the neutrons from the γs.

The calibrated and gated TOF spectra are converted into the neutron energy (E_n) spectra using the following relation:

$$E_n = \frac{1}{2} m_n \frac{l^2}{t^2}, \tag{1}$$

where m_n is the neutron mass, l is the flight path, and t is the TOF. The neutron energy spectra thus obtained are converted from the laboratory frame to the center-of-mass frame. The theoretical neutron energy spectrum of the ^{252}Cf source is obtained using the expression

$$\frac{dN}{dE} = \sqrt{E_n} \exp\left(-\frac{E_n}{T}\right), \tag{2}$$

where $T = 1.3$ MeV for ^{252}Cf [21]. The energy-dependent efficiency of the neutron detectors are obtained by comparing the experimental and theoretical neutron energy spectra. The experimentally obtained efficiencies are then compared with the Monte Carlo simulation from the computer code MODEFF [22]. A good agreement is observed between the experimental and the simulated efficiencies of the neutron detectors as shown in Fig. 5.

B. Extraction of neutron multiplicity

To extract neutron multiplicities for different reactions, the recorded TOF spectra are used to obtain the energy spectra following the procedure described in the last section.

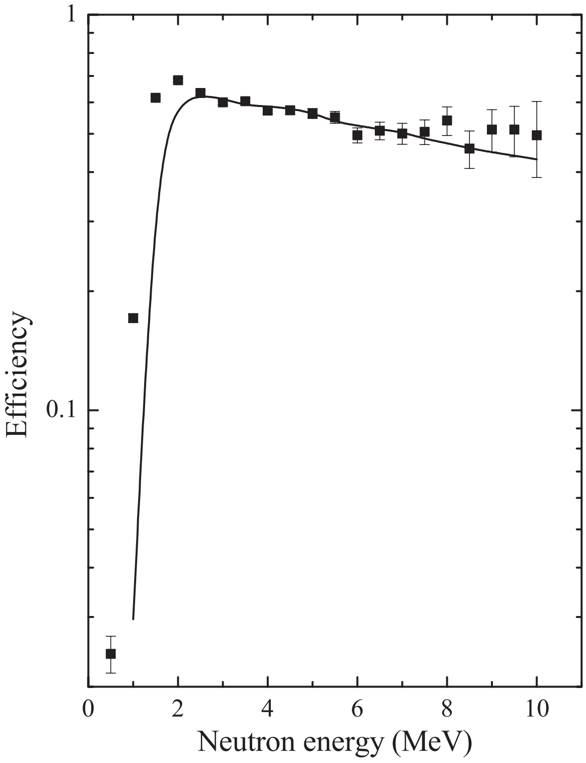

FIG. 5. Comparison of the experimentally obtained neutron efficiency (filled square) with the same obtained using Monte Carlo simulation code MODEFF (solid line) at 120 keV electron equivalent detection threshold.

The neutron energy spectra thus obtained are then corrected with the experimentally obtained energy-dependent neutron detection efficiency.

The neutron energy spectra can have contributions from the following four sources: (1) emission from the compound nucleus (CN) (pre-scission), (2) emission from one of the fission fragments (FF) (post-scission), (3) emission from the complementary fragment (FF) (post-scission), and (4) emission from non-compound-nucleus processes (NCN).

In the literature, it is observed that the lowest value of $z_p z_t$, where the NCN processes come into the picture, is 736 [23,24]. Since the $z_p z_t$ value for the systems under study is 702 and is close to the above value, the folding angle distribution of the fission fragments has been studied carefully for assessing the contribution of NCN processes. For this study, the position information of the fission fragments obtained by calibrating the position spectra is used. The X and Y positions are converted into polar (θ) and azimuthal (ϕ) angles. The polar and azimuthal folding angle distributions for all the reactions, at the beam energy range under study, are found to be Gaussian as shown in Fig. 6. The values of the folding angles obtained experimentally are found to be in agreement with the folding angles calculated using a full momentum transfer process. This confirms that compound nuclear fission is the dominating process, whereas the non-compound-nuclear processes are negligible.

Neglecting the contribution from the NCN processes, the neutron multiplicities can be expressed as the sum of the

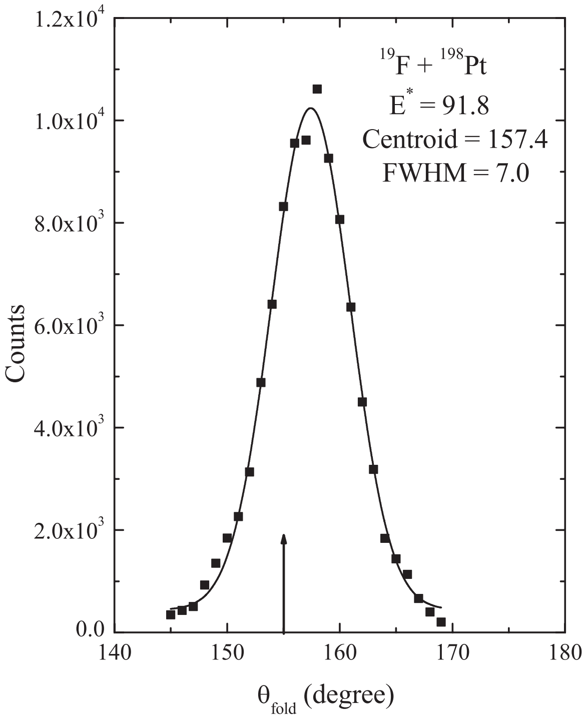

FIG. 6. Folding angle distribution (filled square) of fission fragments for the reaction of $^{19}\mathrm{F} + {}^{198}\mathrm{Pt}$ at 140.8 MeV. Line shows the Gaussian fit to the distribution and the arrow marks the folding angle calculated assuming a full momentum transfer process.

contributions of three moving neutron sources. The neutron multiplicities and the temperatures (T) are assumed to be the same for both the fission fragments. Hence, the total neutron multiplicity can be given as

$$M_{\mathrm{total}} = M_{\mathrm{pre}} + 2M_{\mathrm{post}}, \tag{3}$$

where M$_{\mathrm{pre}}$ and M$_{\mathrm{post}}$ are the pre-scission and the post-scission neutron multiplicities, respectively. The energy spectra of all the neutron detectors are then simultaneously fitted with the theoretical expression for particle spectra from moving sources (Watt expression) [25] where M_{pre}, M_{post}, T_{pre}, and T_{post} appear as free parameters.

The values M_{pre}, M_{post}, T_{pre}, and T_{post} obtained for different CN are given in Tables I–III, and Fig. 7 shows the fitted plots along with contributions from different neutron sources.

From Fig. 7, it is clear that the shape-contributions for different sources vary dramatically with the correlation angle between the neutron sources and the detectors. The variation is mainly because of kinematic focusing effects on the neutrons emitted from the rapidly moving fission fragments. Figure 8 shows the angular distribution of neutrons, where the differential neutron yield resulting from the integration of neutron energy spectra from 0 to 6 MeV versus the neutron detector angle for the in-plane detectors are plotted. The results are also compared with the sum of the contributions from different sources of neutrons obtained from the moving source fitting. The contributions from the individual sources is also shown (see Fig. 8). It is observed that the summed spectra contain two peaks representing the two neutron sources (fission fragments). The neutron contribution from individual fission fragments is Gaussian with a peak around the detector center, and the contribution of the CN is also a Gaussian, peaking at 0°. It confirms the kinematical focusing of neutrons in the direction of the emitting sources.

The total neutron multiplicities (M_{total}) are also compared with the energy balance equation following the prescription suggested by Hinde *et al.* [8]. According to this prescription, the total available decay energy can be obtained using two different methods. One is based on the initial excitation energy of the CN. Here, the total available decay energy is given as

$$E_x(f) = E_{\mathrm{c.m.}} + Q(f) - E_K \tag{4}$$

where $E_{\mathrm{c.m.}}$ is center-of-mass energy, $Q(f)$ is the Q value of the fission reaction, and E_K is the total kinetic energy of the fragments. In the other method, the experimentally obtained M_{total} is used. In this case, the total available decay energy is given as

$$E_x(f) = E_\gamma(f) + \sum_{i=1}^{M_{\mathrm{total}}} \left(8.07 + E_n^i\right), \tag{5}$$

where $E_\gamma(f)$ is the excitation energy carried away by γ emission, 8.07 is the mass defect of a neutron in MeV, and E_n^i is the kinetic energy of the emitted neutron. If the total available decay energies obtained by both prescriptions match within ±5 MeV, then one can say that the experimentally obtained multiplicities are consistent with the initial excitation energies of the CN. It is observed for the present systems that the experimental multiplicities are consistent with the available

TABLE I. Values of M_{pre}, M_{post} M_{total}, T_{pre}, and T_{post} for the $^{19}\mathrm{F} + {}^{198}\mathrm{Pt}$ system.

E$_{\mathrm{lab}}$ (MeV)[a]	E^* (MeV)	M_{pre}	M_{post}	M_{total}	T_{pre}	T_{post}
90.2	46.6	2.44 ± 0.12	0.82 ± 0.045	4.08 ± 0.15	1.01 ± 0.040	0.97 ± 0.035
96.2	52.0	2.70 ± 0.12	0.77 ± 0.045	4.24 ± 0.15	1.11 ± 0.040	1.01 ± 0.044
103.0	58.2	2.96 ± 0.12	0.97 ± 0.045	4.90 ± 0.15	1.13 ± 0.034	1.04 ± 0.039
107.1	62.0	3.24 ± 0.13	0.94 ± 0.047	5.12 ± 0.16	1.19 ± 0.035	1.03 ± 0.041
113.1	67.5	3.64 ± 0.15	0.98 ± 0.050	5.60 ± 0.18	1.26 ± 0.036	1.08 ± 0.047
120.2	74.0	4.06 ± 0.18	1.05 ± 0.094	6.16 ± 0.26	1.42 ± 0.040	1.10 ± 0.060
126.8	80.0	4.56 ± 0.19	0.75 ± 0.096	6.06 ± 0.27	1.52 ± 0.080	1.12 ± 0.050
133.4	86.0	5.05 ± 0.20	0.75 ± 0.112	6.55 ± 0.30	1.56 ± 0.070	1.14 ± 0.060
139.6	91.8	5.52 ± 0.20	0.80 ± 0.066	7.12 ± 0.24	1.61 ± 0.040	1.17 ± 0.055

[a] Corrected for energy loss in the target.

TABLE II. Values of M_{pre}, M_{post}, M_{total}, T_{pre}, and T_{post} for the $^{19}\text{F} + {}^{196}\text{Pt}$ system.

E_{lab} (MeV)[a]	E^* (MeV)	M_{pre}	M_{post}	M_{total}	T_{pre}	T_{post}
90.6	48.1	2.37 ± 0.11	0.83 ± 0.043	4.03 ± 0.14	1.00 ± 0.040	1.03 ± 0.036
96.6	53.6	2.61 ± 0.12	0.81 ± 0.045	4.22 ± 0.15	1.06 ± 0.040	1.05 ± 0.041
105.8	62.0	3.10 ± 0.13	0.94 ± 0.047	4.98 ± 0.16	1.21 ± 0.036	1.09 ± 0.042
111.8	67.5	3.35 ± 0.14	0.99 ± 0.048	5.33 ± 0.17	1.31 ± 0.066	1.14 ± 0.060
120.5	75.4	3.96 ± 0.20	0.93 ± 0.083	5.82 ± 0.26	1.35 ± 0.043	1.17 ± 0.050
127.1	81.4	4.51 ± 0.22	0.90 ± 0.078	6.31 ± 0.27	1.47 ± 0.060	1.19 ± 0.06
133.7	87.4	5.09 ± 0.17	0.87 ± 0.098	6.82 ± 0.26	1.50 ± 0.070	1.22 ± 0.06
138.5	91.8	5.26 ± 0.20	1.12 ± 0.098	7.50 ± 0.28	1.55 ± 0.060	1.23 ± 0.05

[a] Corrected for energy loss in the target.

excitation energies of the compound nuclei, as shown in Fig. 9.

IV. STATISTICAL MODEL ANALYSIS

The experimentally obtained neutron multiplicities are compared with the statistical model predictions. In these calculations, emission of neutrons, protons, αs, and giant dipole resonance (GDR) γ rays are considered along with fission as the possible decay channels of a compound nucleus. The light particle and the γ decay widths are obtained from the Weisskopf formula [5].

The fission width in the present work is taken from Ref. [12] where the effect of dissipation is included. Considering fission as a diffusive process of a Brownian particle across the fission barrier in a viscous medium, Kramers solved the relevant Fokker-Planck equation and obtained the following expression for fission width [12] as

$$\Gamma_K = \frac{\hbar\omega_{\text{g.s.}}}{2\pi} e^{-\frac{V_B}{T}} \left[\sqrt{1+\left(\frac{\beta}{2\omega_{\text{sad}}}\right)^2} - \frac{\beta}{2\omega_{\text{sad}}}\right], \tag{6}$$

where β is the reduced dissipation coefficient, $\omega_{\text{g.s.}}$ and ω_{sad} are the local frequencies of the harmonic oscillator potentials which have the same curvatures as the LDM nuclear potential at the ground state and the saddle configuration, respectively. The fission barrier and the nuclear temperature are denoted by V_B and T, respectively. The nuclear potential is obtained as a function of elongation using the finite range liquid drop model (FRLDM) [26]. Since the potential profile depends on the spin of the compound nucleus, the frequencies $\omega_{\text{g.s.}}$ and ω_{sad} should have spin dependences [27,28]. Accordingly, spin dependence of the frequencies is taken into account in the present calculation.

The fission width reaches its stationary value [Eq. (6)] after the elapse of a buildup or transient time τ_f [29] and the dynamical fission width is given as [30]

$$\Gamma_f(t) = \Gamma_K\left[1-\exp\left(-\frac{2.3t}{\tau_f}\right)\right], \tag{7}$$

which is used in the time evolution of the CN in the present calculation.

The particle and γ decay widths and the compound-nuclear temperature are calculated using the level density parameter taken from the work of Ignatyuk *et al.* [15] which takes into account the nuclear shell structure effect at low excitation energies and is given as

$$a(E^*) = \bar{a}\left(1+\frac{f(E^*)}{E^*}\delta W\right), \tag{8}$$

with

$$f(E^*) = 1 - e^{-\frac{E^*}{E_D}}, \tag{9}$$

where $\bar{a}$ is the asymptotic value to which the level density parameter approaches with an increase in excitation energy (E^*) of the CN, δW is the shell correction obtained from the difference between the experimental and LDM masses, and E_D is a damping term which accounts for the washing out of the shell effect with increasing excitation energy. The value of E_D is taken to be 18.5 MeV [31].

TABLE III. Values of M_{pre}, M_{post}, M_{total}, T_{pre} and T_{post} for the $^{19}\text{F} + {}^{194}\text{Pt}$ system.

E_{lab} (MeV)[a]	E^* (MeV)	M_{pre}	M_{post}	M_{total}	T_{pre}	T_{post}
90.6	49.8	1.91 ± 0.10	0.95 ± 0.042	3.81 ± 0.13	1.13 ± 0.042	1.01 ± 0.034
96.6	55.3	2.13 ± 0.10	0.90 ± 0.042	3.93 ± 0.13	1.19 ± 0.040	1.03 ± 0.038
104.0	62.0	2.63 ± 0.10	0.95 ± 0.042	4.53 ± 0.13	1.32 ± 0.037	1.08 ± 0.037
110.0	67.5	2.87 ± 0.20	1.04 ± 0.066	4.95 ± 0.24	1.36 ± 0.060	1.16 ± 0.050
117.2	74.0	3.37 ± 0.19	1.04 ± 0.045	5.45 ± 0.21	1.49 ± 0.040	1.19 ± 0.060
123.7	80.0	3.90 ± 0.21	1.04 ± 0.058	5.98 ± 0.24	1.56 ± 0.060	1.22 ± 0.050
130.3	86.0	4.45 ± 0.20	0.90 ± 0.066	6.25 ± 0.24	1.57 ± 0.100	1.23 ± 0.040
136.7	91.8	4.71 ± 0.19	1.12 ± 0.055	6.95 ± 0.22	1.62 ± 0.040	1.24 ± 0.060

[a] Corrected for energy loss in the target.

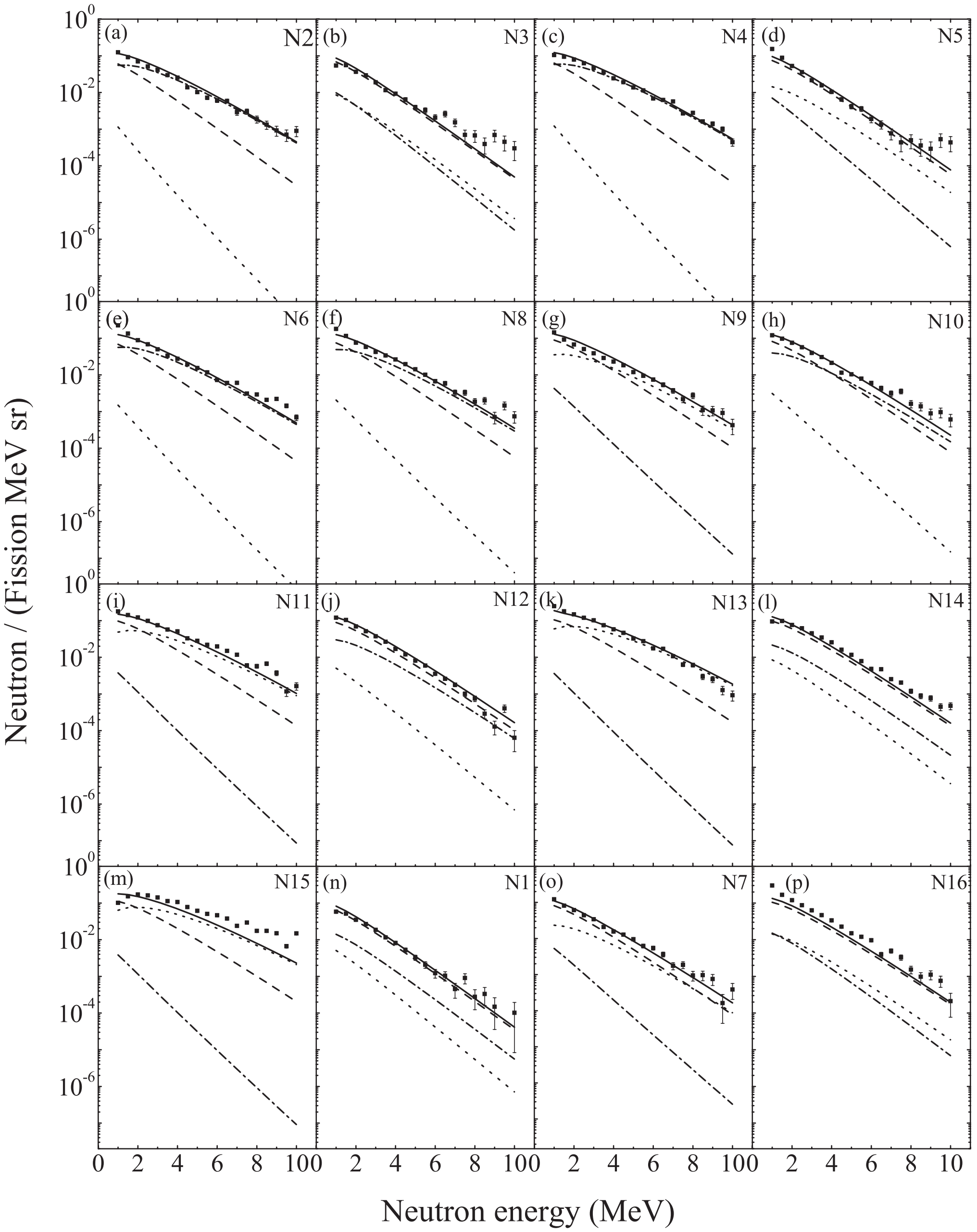

FIG. 7. Neutron multiplicity (filled squares) for the $^{19}\mathrm{F}+{}^{198}\mathrm{Pt}$ system at 52.0 MeV excitation energy for different neutron detectors (N1 to N16). The fits for the pre-scission (dashed lines) and post-scission contribution from one fragment (dotted lines) and that from the other (dash-dotted lines) are also shown. The solid lines represent the sums of the different contributions.

Shell correction can also be added to the fission barrier as follows [15,32]. The parametrized form of the shell-corrected temperature-dependent barrier is given by

$$V_B(T) = V_{\mathrm{LDM}} - \delta W e^{-(E^*/E_D)}, \tag{10}$$

where V_{LDM} is the fission barrier from the finite-range rotating LDM potential [26], E^* is the CN excitation energy, and E_D is the shell damping term.

In the Monte Carlo simulation of compound nuclear decay using various decay widths, the number of neutrons emitted during the transition from the saddle to the scission configuration is also calculated for fission events. The time interval for transition of the CN from saddle to scission is given as [33]

$$\tau_{\mathrm{ss}} = \tau_{\mathrm{ss}}^{o}\left[\sqrt{1+\left(\frac{\beta}{2\omega_{\mathrm{sad}}}\right)^2}+\frac{\beta}{2\omega_{\mathrm{sad}}}\right], \tag{11}$$

where τ_{ss}^{o} is the nondissipative time interval for transition from saddle to scission and its value is taken from Ref. [34]. The neutrons emitted during the saddle-to-scission journey of a CN contribute to the pre-scission neutron multiplicity. The post-scission neutron multiplicities from the fission fragments are also calculated assuming symmetric fission.

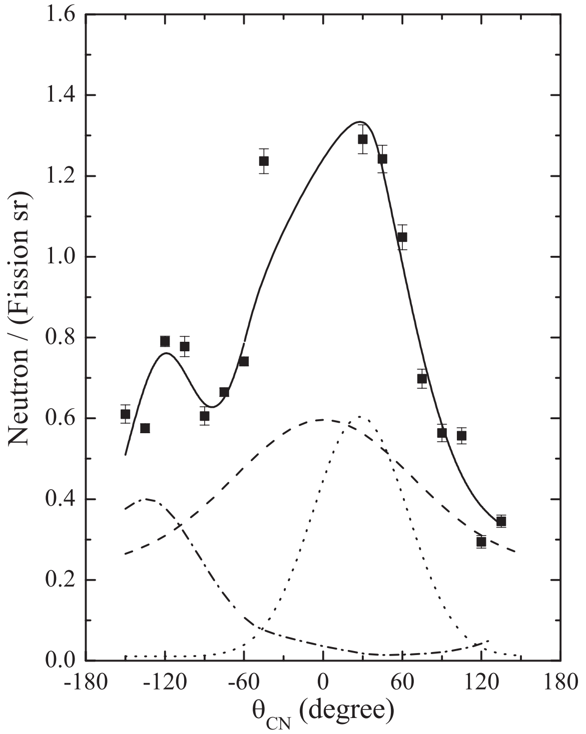

FIG. 8. Experimental neutron angular distribution (solid squares) along with the theoretically obtained angular distribution (solid line). Also shown are the angular distributions of different sources: CN (dashed line), fragment1 (dotted line), fragment2 (dash dotted line).

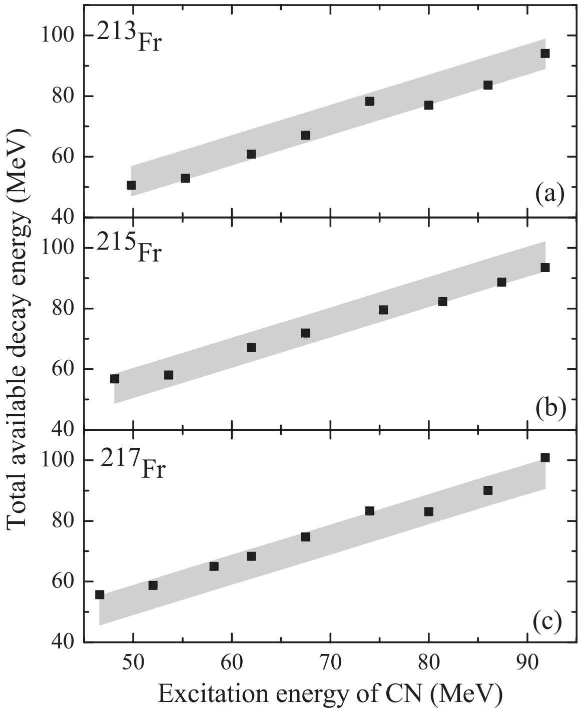

FIG. 9. Total available decay energy vs excitation energy of CN calculated using experimental M_{total} [Eq. (6)] are shown as solid squares, and the shaded areas represent the total available decay energy calculated using excitation energy [Eq. (5)] with a spread of ±5 MeV.

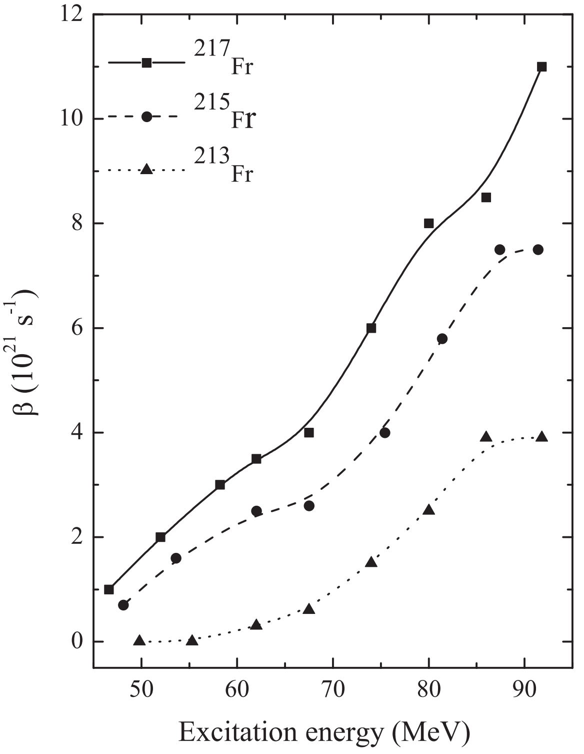

FIG. 10. Excitation energy dependence of β required to fit the experimentally obtained M_{pre} for different systems using LDM masses and without shell corrections in fission barrier. The lines are drawn to guide the eye.

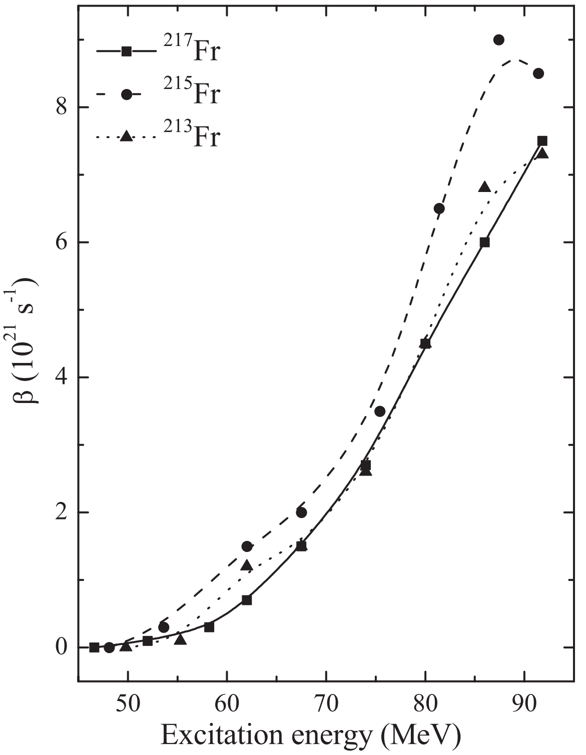

FIG. 11. Excitation function of β values required to fit experimentally obtained M_{pre} using the shell-corrected LDM mass and without shell corrections in the fission barrier for different isotopes of Fr. The lines are drawn to guide the eye.

We first perform statistical model calculations using LDM nuclear masses to obtain the neutron binding energies and the FRLDM for the fission barrier. No shell corrections are applied either to the neutron binding energies or to the fission barrier. The pre-scission neutron multiplicity at each excitation energy is fitted by adjusting the strength of the reduced dissipation coefficient β. It is observed that the experimental data cannot be fitted with a constant value of β and Fig. 10 shows the best-fit β values for different isotopes of Fr. It is observed that the dissipation coefficients for ^{217}Fr and ^{215}Fr isotopes increase fast with increasing excitation energy over its entire range, whereas the dissipation strength remains nearly zero till 70 MeV of excitation energy followed by a slower rate of increase for ^{213}Fr. The overall magnitude of the dissipation strength also remains much smaller for ^{213}Fr than for the other two isotopes of Fr.

We next incorporate the ground-state shell corrections [35] in the liquid-drop-model masses in the statistical model calculations. Figure 11 shows the dissipation strengths required to fit the experimental multiplicities for all three Fr isotopes. It is clearly observed in Fig. 11 that the anomalous lowering of dissipation strength for ^{213}Fr disappears and all the isotopes require nearly the same dissipation strength to fit the experimental results. This observation can be explained as follows. Since the masses are taken to be the sum of the LDM masses and the shell corrections, the neutron separation energy obtained from the shell-corrected LDM masses increases for ^{213}Fr compared to that from the LDM masses while it decreases for the other two isotopes. This reduces the M_{pre} values for ^{213}Fr, but increases the M_{pre} for ^{217}Fr and ^{215}Fr for a given value of the dissipation strength in the statistical model calculation. Consequently, higher values of dissipation strength are required to fit the M_{pre} for ^{213}Fr; whereas lower values of dissipation are required for the other two isotopes, in comparison to the calculations without shell correction in masses. The dissipation strengths of the different isotopes therefore converge.

The liquid-drop-model masses with shell corrections, however, differ from the experimental ground-state masses to some extent. We therefore use the experimental masses in our next calculation. Figure 12 shows the fitted β values for the three isotopes of Fr. Here also we find the excitation functions of the fitted β values to be nearly the same for all three Fr isotopes.

Comparing the results given in Figs. 10–12, we make an interesting observation here. When shell correction is not applied to the ground-state nuclear masses, the fitted β values for the different Fr isotopes are quite different (Fig. 10). However, the best-fit β values for the three Fr isotopes converge to a common value at each excitation energy when either shell-corrected (Fig. 11) or experimental nuclear masses (Fig. 12) are used in the statistical model calculation. Though it is expected that the calculated M_{pre} values (and hence fitted β values) will change when the input masses are changed in the statistical model calculation for a given compound nucleus, the above observation of the convergence of the fitted β values is made possible only because the present experimental

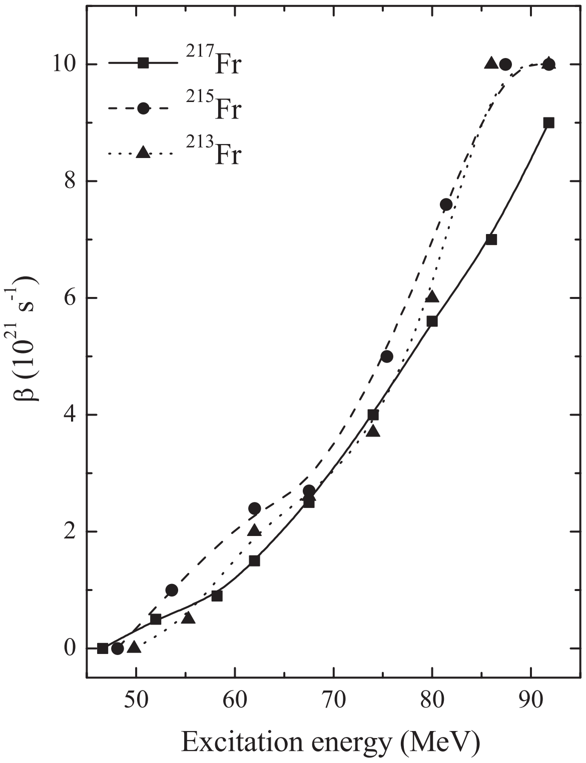

FIG. 12. Excitation function of β values required to fit experimentally obtained M_{pre} using the experimental masses and with no shell corrections in the fission barrier for different isotopes of Fr. The lines are drawn to guide the eye.

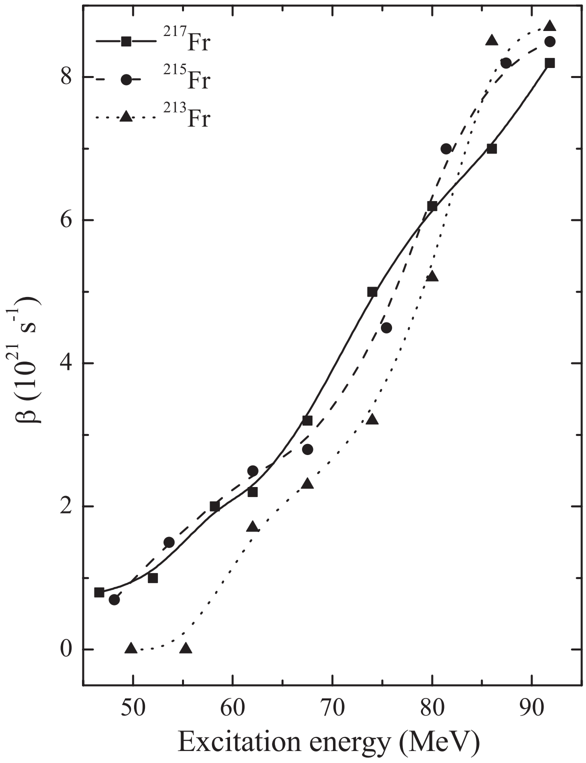

FIG. 13. Excitation function of β values required to fit experimentally obtained M_{pre} using the experimental mass and shell-corrected fission barrier for different isotopes of Fr. The lines are drawn to guide the eye.

measurements are made for an isotopic sequence of compound nuclei.

We now investigate the effect of shell correction to the fission barrier on the fitted values of dissipation strength. To this end, we compare the excitation function of the fitted β obtained without shell correction to the fission barrier (Fig. 12) with that obtained with the shell-corrected fission barrier (Fig. 13). Experimental nuclear masses are used in both calculations and the latter was obtained in an earlier work [18]. It is observed that inclusion of the shell effect in the fission barrier affects the fitted β values differently for closed-shell and non-closed-shell nuclei at low excitation energies. However, the effect of including the shell correction in the fission barrier is not as severe as the effect of the shell correction in LDM masses (Figs. 10 and 11) or the effect of shell correction in the level density formula [18].

V. SUMMARY AND CONCLUSIONS

The pre- and post-scission neutron multiplicity excitation functions are experimentally measured for three isotopes of Fr which are formed as compound nuclei in fusion-fission reactions and one of the compound nuclei has a major neutron shell closure. The experimental neutron multiplicities are compared with the statistical model predictions using the fission width due to Kramers. The best-fit β values of the different nuclei are found to be quite different when no shell effects are included in the nuclear masses or the fission barriers (Fig. 10). In particular, the β values for the closed-shell ^{213}Fr nucleus are much smaller than those of the other two non-closed-shell nuclei. However, when the shell-corrected nuclear masses or the experimental nuclear masses are used in the calculations, the divergence among the β values of the three nuclei disappears to a large extent (Figs. 11 and 12). This clearly demonstrates the importance of using the correct neutron binding energy in the neutron width calculation in order to extract the dissipation strength from fitting experimental neutron multiplicity.

A difference between the magnitudes of β values of closed-shell and non-closed-shell nuclei, however, appears at low excitation energies, when a shell correction is incorporated in the fission barrier. Shell correction in the fission barrier, however, does not affect the fitted values of the dissipation coefficient as strongly as is found when including shell effects in nuclear masses or in the level density parameter.

ACKNOWLEDGMENTS

The authors thank the accelerator groups (LINAC and Pelletron) of IUAC, New Delhi, for providing beams of excellent quality throughout the experiment. The authors are grateful to Dr. A. Roy for his constant encouragement during the entire duration of the project. Thanks are also due to R. P. Singh, P. Barua, and M. Oswal for their help at various stages of the experiment. The financial support from the Council of Scientific and Industrial Research (CSIR), Government of India, in terms of a Shyama Prasad Mukherjee Fellowship (SPMF) to one of the authors (V.S.) is gratefully acknowledged. B.R.B. acknowledges the Department of Atomic Energy (DAE), Government of India, for a DAE young scientist research grant (YSRA). The calculations were performed at the high-performance computing center (HPCC) of the Department of Physics, Panjab University, Chandigarh.

---

[1] A. J. Sierk, S. E. Koonin, and J. R. Nix, Phys. Rev. C **17**, 646 (1978).

[2] W. J. Swiatecki, J. Phys. Suppl. **33**, C5-45 (1972).

[3] K. T. R. Davies, A. J. Sierk, and J. R. Nix, Phys. Rev. C **13**, 2385 (1976).

[4] D. H. E. Gross and H. Kalinowski, Phys. Rep. **45**, 175 (1978).

[5] P. Frobrich and I. I. Gontchar, Phys. Rep. **292**, 131 (1998).

[6] D. Hilscher and H. Rossner, Ann. Phys. (Paris) **17**, 471 (1992).

[7] M. Thoennessen and G. F. Bertsch, Phys. Rev. Lett. **71**, 4303 (1993).

[8] D. J. Hinde, R. J. Charity, G. S. Foote, J. R. Leigh, J. O. Newton, S. Ogaza, and A. Chattejee, Nucl. Phys. A **452**, 550 (1986).

[9] J. O. Newton, D. J. Hinde, R. J. Charity, J. R. Leigh, J. J. M. Bokhorst, A. Chatterjee, G. S. Foote, and S. Ogaza, Nucl. Phys. A **483**, 126 (1988).

[10] Peter Paul and Michael Thoennessen, Annu. Rev. Nucl. Part. Sci. **44**, 65 (1994).

[11] B. B. Back, D. J. Blumenthal, C. N. Davids, D. J. Henderson, R. Hermann, D. J. Hofman, C. L. Jiang, H. T. Penttila, and A. H. Wuosmaa, Phys. Rev. C **60**, 044602 (1999).

[12] H. A. Kramers, Physica (Amsterdam) **7**, 284 (1940).

[13] Helmut Hofmann and Fedor A. Ivanyuk, Phys. Rev. Lett. **82**, 4603 (1999).

[14] I. Dioszegi, N. P. Shaw, I. Mazumder, A. Hatzikoutelis, and P. Paul, Phys. Rev. C **61**, 024613 (2000).

[15] A. V. Ignatyuk *et al.*, Yad. Fiz. **21**, 485 (1975) [Sov. J. Nucl. Phys. **21**, 255 (1975)].

[16] H. Hofmann, F. A. Ivanyuk, C. Rummel, and S. Yamaji, Phys. Rev. C **64**, 054316 (2001).

[17] J. Blocki, Y. Boneh, J. R. Nix, J. Randrup, M. Robel, A. J. Sierk, and W. J. Swiatecki, Ann. Phys. (NY) **113**, 330 (1978).

[18] Varinderjit Singh, B. R. Behera, Maninder Kaur, P. Sugathan, K. S. Golda, A. Jhingan, Jhilam Sadhukhan, Davinder Siwal, S. Goyal, S. Santra, A. Kumar, R. K. Bhowmik, M. B. Chatterjee, A. Saxena, Santanu Pal, and S. Kailas, Phys. Rev. C **86**, 014609 (2012).

[19] T. G. Masterson, Nucl. Instrum. Methods **88**, 61 (1970).

[20] S. Venkataramanan, Arti Gupta, K. S. Golda, Hardev Singh, Rakesh Kumar, R. P. Singh, and R. K. Bhowmik, Nucl. Instrum. Methods A **596**, 248 (2008).

[21] E. A. Lorch, Int. J. Appl. Rad. Isotop. **24**, 585 (1973).

[22] R. A. Cecil, B. D. Anderson, and R. Madey, Nucl. Instrum. Methods **161**, 439 (1979).

[23] D. J. Hinde, M. Dasgupta, J. R. Leigh, J. P. Lestone, J. C. Mein, C. R. Morton, J. O. Newton, and H. Timmers, Phys. Rev. Lett. **74**, 1295 (1995).

[24] D. J. Hinde, M. Dasgupta, J. R. Leigh, J. C. Mein, C. R. Morton, J. O. Newton, and H. Timmers, Phys. Rev. C **53**, 1290 (1996).

[25] D. Hilscher, J. R. Birkelund, A. D. Hoover, W. U. Schroder, W. W. Wilcke, J. R. Huizenga, A. C. Mignerey, K. L. Wolf, H. F. Breuer, and V. E. Viola, Phys. Rev. C **20**, 576 (1979).

[26] A. J. Sierk, Phys. Rev. C **33**, 2039 (1986).

[27] J. Sadhukhan and S. Pal, Phys. Rev. C **78**, 011603(R) (2008).

[28] J. P. Lestone and S. G. McCalla, Phys. Rev. C **79**, 044611 (2009).

[29] P. Grange, Li Jun Qing, and H. A. Weidenmuller, Phys. Rev. C **27**, 2063 (1983).

[30] K. H. Bhatt, P. Grange, and B. Hiller, Phys. Rev. C **33**, 954 (1986).

[31] W. Reisdorf, Z. Phys. A **300**, 227 (1981).

[32] Y. Aritomo, Nucl. Phys. A **780**, 222 (2006).

[33] H. Hofmann and J. R. Nix, Phys. Lett. B **122**, 117 (1983).

[34] P. Grange, S. Hassani, H. A. Weidenmuller, A. Gavron, J. R. Nix, and A. J. Sierk, Phys. Rev. C **34**, 209 (1986).

[35] W. D. Myers and W. J. Swiatecki, Nucl. Phys. A **601**, 141 (1996).